A Benchmark Study of Aromaticity Indexes for Benzene, Pyridine, and the Diazines - II. Excited State Aromaticity

Pedersen, Jacob; Mikkelsen, Kurt V.

Published in:
Journal of Physical Chemistry A

Link to article, DOI:
10.1021/acs.jpca.2c07059

Publication date:
2022

Document Version
Peer reviewed version

A benchmark study of aromaticity indexes for benzene, pyridine and the diazines - II. Excited state aromaticity

Jacob Pedersen[†,ξ],
Kurt V. Mikkelsen[†*]
[†]Department of Chemistry, University of Copenhagen,
Copenhagen, DK-2100, Denmark
[ξ]Department of Chemistry, Technical University of Denmark,
Kongens Lyngby, DK-2800, Denmark
[*]kmi@chem.ku.dk

April 2, 2024

Abstract

In this work, one geometrical aromaticity index and four electron sharing indexes are benchmarked for their application in excited state aromaticity calculations. Two computational feasible and reliable procedures are identified, namely, CAM-B3LYP/cc-pVTZ and ωB97X-D/cc-pVTZ. Topological effects on the first excited singlet and triplet electronic manifold were investigated, and the latter was in general found to display more aromatic character compared to the S_1 surface. Besides, geometrical relaxation on each of the manifolds was observed to hamper the aromaticity, thereby resulting in more anti-aromatic character. The relative order of excited state aromaticity within the studied molecules was noted to resemble the reversed version of the relative

order of ground state aromaticity. Thereby, the following generalization was postulated; 'the more aromatic a molecule is in its ground state, the more anti-aromatic it will be in its electronic first excited manifolds'.

Keywords: Aromaticity Indexes; Electron Sharing Indexes; Quantum Theory of Atoms in Molecules; Density Functional Theory; Benchmark.

1 Introduction

The notion of aromaticity can be used to predict and explain the stability, reactivity and various magnetic properties of molecules.[1] Aromaticity exists in many forms; e.g. Hückel aromaticity, in-plane aromaticity, Möbius aromaticity and excited state aromaticity.[2,3] Nonetheless, no general accepted definition of aromaticity exists; therefore, aromaticity is extremely difficult to quantify. Consequently, various definitions have been formulated over the past decades all centered on different physicochemical properties and structural requirements.[4] The formulation of an unique and proper definition of aromaticity is complicated by the fact, that aromaticity is not a measurable quantity. Instead, it must be quantified by indexes designed to scale the aromaticity in a given molecule.[4]

Aromatic molecules are not very reactive compared to their aliphatic counterparts. The delocalization of π-electrons makes the aromatic molecules quite stable and thereby less reactive. However, the opposite is true for anti-aromatic molecules, which are very unstable and therefore highly reactive.[5] The resonance energy is defined as the stabilization energy of the aromatic molecule relative to the expected electronic energy of the corresponding Kekulé structure with alternating single and double bonds.[6] The gain or loss of aromaticity or anti-aromaticity, respectively, might thus be used as a driving force in chemical reactions, since these events are partly controlled by energetic conditions and stability.

Hückel's rule of aromaticity applies for all monocyclic organic molecules in their molecular ground state (S_0). The rule states; if a molecule is cyclic, planar, fully conjugated and contains $4n + 2$ electrons, with n being a natural number ($n \in \mathbb{N}$), the molecule is aromatic.[1–4] A molecule that meets the structural requirements is structurally arranged, such that each atom in the aromatic ring has one p-orbital perpendicular to the molecular plane. This parallelization of p-orbitals allows for the delocalization of π-electrons and thereby resonance between the π-bonds. If a molecule, on the other hand, satisfies the three first conditions but only contains $4n$ electrons, the molecule is anti-aromatic. Moreover, molecules that fail to meet two or more of the conditions are classified as non-aromatic. Hückel's rule was later on extended to include polycyclic hydrocarbons by Clar's rule.[7,8] It is noted, however, that non-planar systems, such as Möbious topologies, migth be aromatic, although they do not follow Hückel's rule of aromaticity.[9]

Baird presented in 1972 rules for the prediction of aromaticity and anti-aromaticity on the first excited electronic triplet state (T_1) on the basis of orbital interactions and energy differences.[10] In particular, Baird defined two types of orbital interactions, namely, type I and type II interactions. Type I interactions occur between two singly occupied molecular orbitals, whereas type II interactions occur between singly occupied and doubly occupied or vacant molecular orbitals. Thereby, Baird calculated the bonding energies by these orbital interactions and compared them to their reference structures. The investigated molecules were annulenes, and the reference structures constituted two stable monoradicals, which were made by splitting these annulenes theoretically.[10] The outcome of this study is known as Baird's rule. In general, it predicts that annulenes with $4n$ electrons are aromatic and those with $4n + 2$ electrons are anti-aromatic.[10] This is the exact opposite of Hückel's rule.

The ground state and excited state aromaticity in cyclobutadiene, benzene[11] and cyclooctatetraene[12] have been investigated. In particular, Karadakov computed benzene to be anti-aromatic in its electronically first excited singlet (S_1) and T_1 state.[11] This is in agreement with Baird's rule. Meanwhile, benzene is an aromatic molecule

in its electronic ground state according to Hückel's rule. This reversal of aromaticity in the first excited electronic manifolds relative to the molecular ground state might be beneficial in e.g. artificial photosynthesis research.[13] Skov et al. has recently showed, how the switching properties in benzannulated derivatives of the dihydroazulene-vinylheptafulvene (DHA-VHF) photoswitch[14] get hampered due to loss of aromaticity upon photoexcitation.[15]

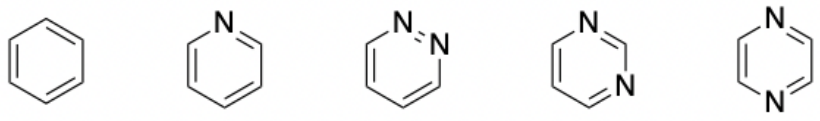

Figure 1: Kekulé structures of benzene (left), pyridine, pyridazine (middle), pyrimidine and pyrazine (right).

Before such build-in aromaticity effects in photoexcitation and -isomerization reactions can be utilized beneficially, a computational feasible and reliable procedure must first be determined. In the first paper of this series, paper I,[16] the five aromaticity indexes; HOMA,[17,18] PDI,[19] MCI,[20] AV1245[21] and FLU[22,23] were benchmarked with respect to ground state aromaticity. In this work, however, the benchmark of aromaticity indexes is extended to include the first excited singlet and triplet states. The set of molecules benchmarked in paper I include benzene, pyridine and the diazines (Fig. 1). Feixas et al. has previously demonstrated, that this set of molecules is highly challenging for most aromaticity descriptors,[24] but because of their resemblance in polycyclic arenes and heteroarenes, they constitute a very representative compound test bed. It was found in paper I, quite surprisingly, that the correlated wavefunction methods failed to describe the aromaticity of the molecules. The DFT methods, ωB97X-D,[25] CAM-B3LYP[26] and M06-2X[27] in combination with a triple-ζ basis set, were, on the other hand, observed to predict reasonable amounts of aromaticity and perform consistently. Consequently, they were concluded to offer the best description of ground state aromaticity.[16]

In regard to photoexcitation reactions, the unrelaxed and relaxed structure of the molecule on the corresponding excited manifold constitute two important geometries. Topological effects on aromaticity indexes with respect to the potential energy surfaces have been reported by Skov et al. recently.[15] However, because the set of molecules studied in this work represents the most common building blocks in polycyclic arenes and heteroarenes, an investigation of the gain or loss of aromaticity within these molecules upon relaxation might offer crucial information for future designs. In the context of artificial photosynthesis research, much attention has been directed towards solar batteries, such as molecular solar thermal (MOST) energy storage systems,[28–30] in which aromaticity reversal between electronic manifolds is hoped to extend storage lifetime, increase energy density, and enhance switching abilities of the photoswitch in otherwise energetically unfavorable photoisomerization reactions.[13,15]Consequently, the aromaticity indexes are calculated with respect to the unrelaxed and relaxed structures for both the S_1 and T_1 manifold in the present work. In respect to the former structures, the HOMA index becomes redundant, since the unrelaxed excited state geometries are equivalent to the optimized ground state geometry.

An overview of the applied aromaticity indexes and the theory behind the wavefunction partition is provided in paper I. In brief, the harmonic oscillator model of aromaticity (HOMA) index describes the equalization of bond lengths that constitute the circuit.[17,18] The other four aromaticity indexes are based upon delocalization of π-electrons; therefore, they are normally called electron sharing indexes (ESI)s.[23] The para-delocalization index (PDI) is an arithmetic average of the delocalization index calculated with respect to all para-related atoms in the aromatic ring.[19] The delocalization index measures the attraction between two basins of attractors.[23] In the context of quantum theory of atoms in molecules (QTAIM),[31,32] each atom acts as an attractor, and the basin of attraction is defined as the region of the phase space, in which the phase points move towards that specific attractor.[33] The multicenter index (MCI) assess the electron delocalization through a summation of all possible permutations of appropriate natural orbital overlap matrix elements,[20] and the large

aromaticity index denoted AV1245 is defined as the arithmetic average of the MCI index for the atoms positioned at the 1st, 2nd, 4th, and 5th position in the circuit, relatively.[21] Lastly, the delocalization-fluctuation (FLU) index assesses the aromaticity by comparing the fluctuation in electron density in between all contiguous atoms with that of corresponding reference bonds.[22,23]

In the following, some potential shortcomings of the applied aromaticity descriptors are noted. The HOMA and FLU index are both based upon reference parameters, for which reason the accuracy of the indexes becomes highly dependent on the selection of these parameters.[18,22] Moreover, together with the PDI and AV1245 index, those four indexes are essentially average values, which means, that important features might get concealed by the less prominent features. This has previously been shown by Casademont-Reig et al. to entail an overestimation of the ground state aromaticity.[34] The PDI is limited to six-membered rings through its definition, thereby reducing its applicability significantly.[19] One inherent limitation of the MCI is the rapid growth in its computational expense with an increasing number of atoms in the molecular circuit.[21]

2 Computational Approach

The geometrical optimized vacuum structures of the molecules calculated at the CAM-B3LYP/cc-pVTZ level of theory from paper I were used as the ground state reference structures. In this context, the optimizations have been carried out with default convergence criteria in Gaussian 16 (Rev. A.03),[35] and the electronic Hessians have all been calculated and checked to be positive-definite to ensure correct geometry minimum.

Next, the excited electronic wavefunctions were calculated with time-dependent density functional theory.[36–41] The first eight excited states were calculated in order to increase the dimensionality of the solution space and thereby the flexibility of the electronic wavefunction. In addition, the singlet and triplet states were requested

in the TD-input on the command line, respectively. The excited state geometry optimization calculations were performed in Gaussian 16 (Rev. A.03) with default convergence criteria, and the electronic Hessians have been calculated and checked to be postive-definite.

In analogue to the computations in paper I, some of the relaxed structures displayed large out-of-plane imaginary normal mode frequencies. This has been speculated to be a consequence of intramolecular basis set superposition errors in paper I. However, since no effects were observed in the aromaticity indexes with respect to the ground state aromaticity calculations nor in the current work, no attempt to correct for these transition structures has been performed. A table over the level of theories that resulted in imaginary normal mode frequencies are provided in the supporting information (SI).

The aforementioned excited state electronic structure calculations have been carried out with the ωB97X-D,[25] CAM-B3LYP[26] and M06-2X[27] DFT functionals each in combination with the cc-pVDZ,[42,43] Def2TZVP[44] and 6-311+G(d)[45,46] basis set. All the electronic structure methods have been employed in their restricted scheme, which have been manually written within the corresponding electronic wavefunction files subsequently.

The AIMAll software package[47] was used for the partitioning of the electronic wavefunction and subsequent topological wavefunction analysis. Details on the AIMAll-calculation settings are provided in paper 1. Finally, the aromaticity indexes were calculated with the ESI-3D program.[48]

3 Results & Discussion

The aromaticity indexes are benchmarked in this section. In addition, the changes in aromaticity with respect to the molecules and topological modifications are assessed and commented upon. On the basis of the benchmark study, the best methods will be recommended for future usage in aromaticity calculations.

3.1 Benchmark

To begin with, the aromaticity indexes calculated with respect to the relaxed structures on the S_1 surface are investigated. Fig. 2 shows the computed aromaticity indexes for the molecules under investigation. In general, the index values fluctuate little with respect to the basis sets. The two basis sets from Dunning and Karlsruhe,

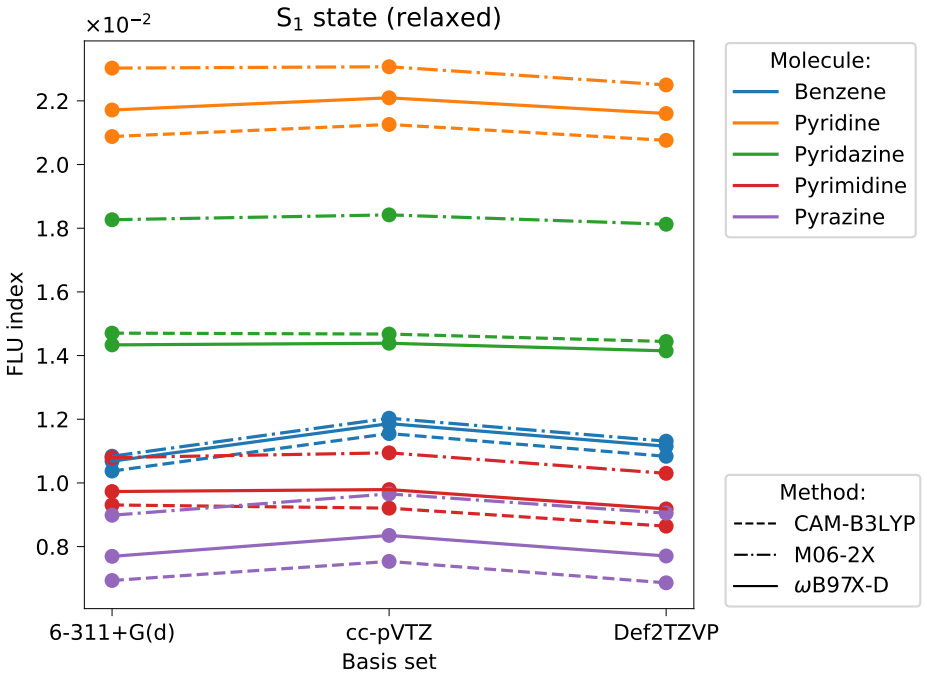

(a) FLU index

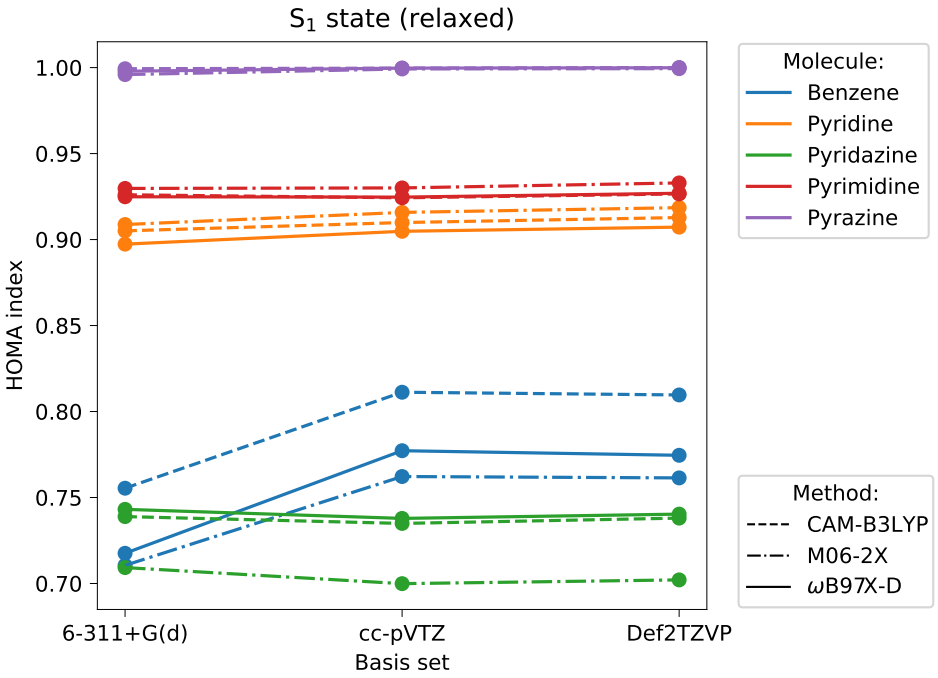

(b) HOMA index

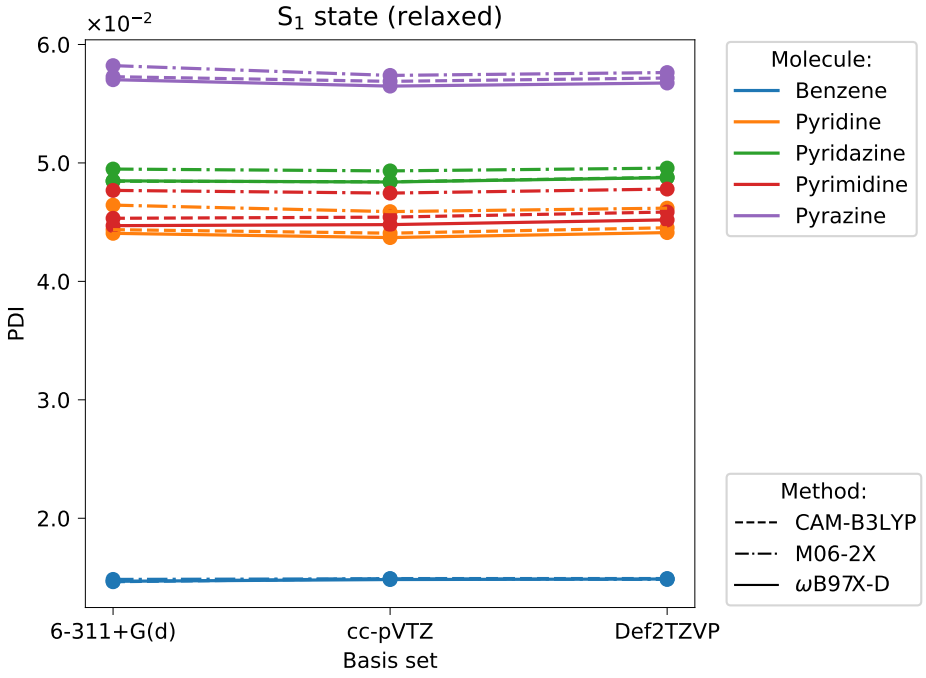

(c) PDI

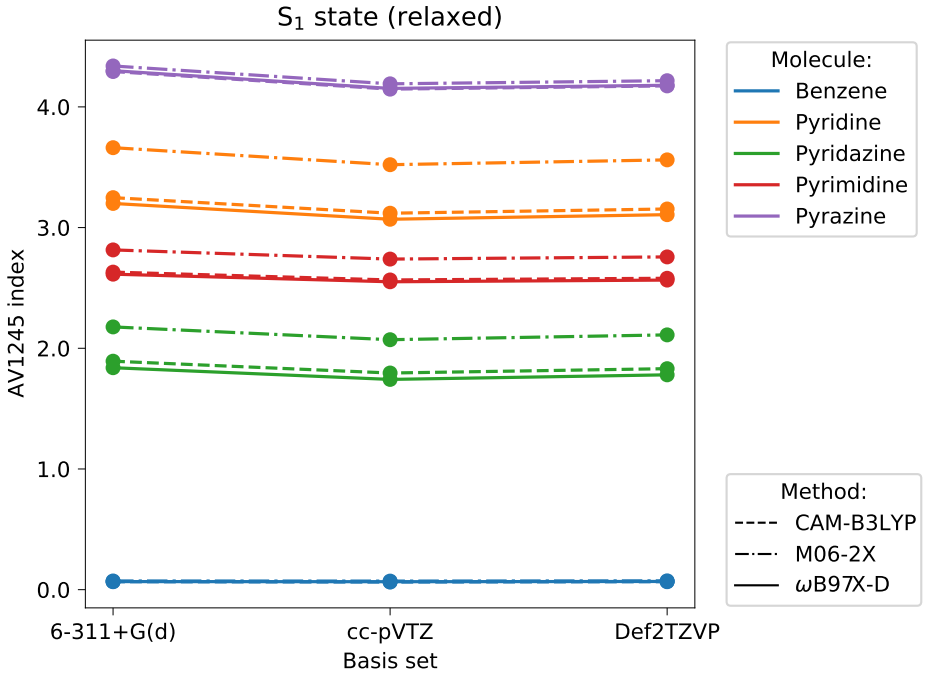

(d) AV1245 index

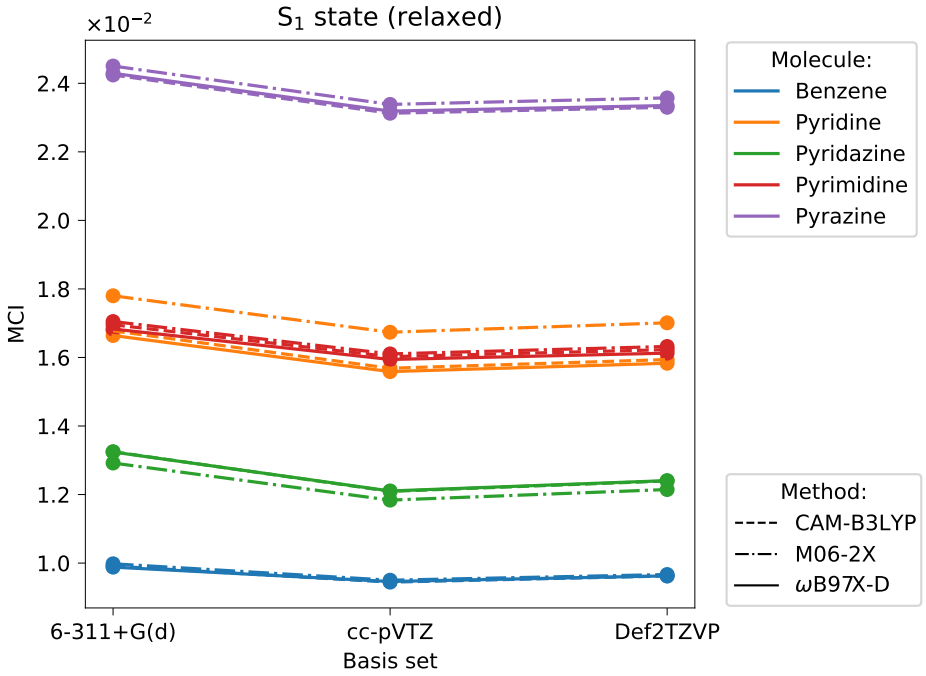

(e) MCI

Figure 2: Benchmark plot of the (a) FLU index, (b) HOMA index, (c) PDI, (d) AV1245 index and (e) MCI calculated on the S_1 surface with respect to the relaxed structures. The methods are specified by the different linestyles, and the molecules are specified by the colours.

cc-pVTZ and Def2TZVP, respectively, are noted to perform almost identical with exception of the FLU index. The triple-ζ Pople style basis set, 6-311+G(d), on the other hand, predicts a little bit larger index values for the PDI, AV1245 index and MCI, and somewhat smaller index values for the HOMA index compared to the other two basis sets. In particular, the largest difference with respect to the basis set dependency is observed for the HOMA index between the 6-311+G(d) basis set and the two other basis sets for benzene. A deviation in this trend is noted for pyridazine. Here, a bit larger index values for the HOMA index are obtained with the 6-311+G(d) basis set.

The similarity in performance of the cc-pVTZ and Def2TZVP basis sets and deviation with respect to the 6-311+G(d) basis set is a consequence of basis set flexibility. Dunning's and Karlsruhe's basis set are much more flexible due to their higher dimensionality and containment of polarization functions with higher angular momentum compared to that within the Pople style basis set. The ESIs, that is, FLU index, PDI, AV1245 index and MCI, are all defined in terms of QTAIM. In this context, the wavefunction partition is carried out in real-space, at which the partition itself becomes independent of the accuracy of the Hilbert space.[31,32] The wavefunction and electron density, however, depend on the basis set, but because of the QTAIM machinery, that is, the wavefunction partition and subsequent basin integration, the effect will not be as prominent in the ESIs as in the HOMA index. This is a consequence of the HOMA index being based upon the bond lengths, which are directly dictated by the accuracy of the potential energy surface and thereby the dimensionality and flexibility of the Hilbert space.

To ensure that the difference between the Pople style basis set and the other two basis sets is not a consequence of the inclusion of diffuse basis functions in the former, the aromaticity indexes have been calculated at the CAM-B3LYP/aug-cc-pVTZ level of theory for pyrazine. The aromaticity indexes are found to be; FLU = 7.28 $\times$ 10^{-3}, HOMA = 1.000, PDI = 5.67 $\times$ 10^{-2}, AV1245 = 4.151, and MCI = 2.32 $\times$ 10^{-2}. These index values are almost identical to the ones computed with the

non-augmented cc-pVTZ basis set with the same DFT method; therefore, the diffuse basis functions' impact on the index values can be outruled. This is in agreement with the findings from paper I, where augmentation of diffuse basis functions were found to cause little to no effect.

In respect to the FLU index, a bit larger index values are in general obtained with the cc-pVTZ basis set compared to the 6-311+G(d) and Def2TZVP basis sets. Besides, the Pople style and Karlsruhe basis sets are noted to perform quite similarly. The cc-pVTZ basis set is contracted using the generalized contraction scheme[49] with the orbital exponents of the incoming primitive basis functions being optimized in correlated calculations.[42,50] Consequently, the cc-pVTZ basis set is capable of describing correlation effects.[51,52] The FLU index is based upon the exchange-correlation density; therefore, the systematic inclusion of correlation effects in the cc-pVTZ basis set causes the larger FLU index values. The exchange-correlation density is defined in paper I.

Conclusively, the aromaticity indexes' basis set dependence is in general low, however, it is most prominent in the FLU index and HOMA index for benzene and pyrazine. Benchmark plots for the unrelaxed structures and the other excited manifold are provided in the SI. Overall, the same tendencies are observed. No reference values are available for the excited state aromaticity indexes. Therefore, the recommendation of basis set is based upon the aforementioned arguments, and the cc-pVTZ basis set is thus concluded to be the preferred choice.

The performances of the DFT methods are elucidated in the following. In analogue to the basis set analysis, the aromaticity indexes computed with respect to the relaxed structures on the S_1 surface are discussed initially. Fig. 2 reveals, that CAM-B3LYP and ωB97X-D perform almost identically. In respect to the FLU index and HOMA index, only a few deviations of this tendency are noted. These differences are attributed to the inclusion of dispersion forces in the ωB97X-D functional. The Minnesota functional, M06-2X, is observed to predict the larger ESI values. On the

other hand, notably smaller index values for the HOMA index are obtained with the Minnesota functional. In particular, the FLU index of pyridazine calculated with M06-2X is approximately 1.83×10^{-2}, whereas both CAM-B3LYP and ωB97X-D predict approximately 1.45×10^{-2}. In light of the threshold for aromaticity and anti-aromaticity with respect to the FLU index being at the 10^{-3} scale,[16] this jump in index value is extremely large. However, in reference to the threshold of aromaticity and anti-aromaticity for the other ESIs,[16] the changes are not significant. In respect to the HOMA index, the changes with respect to the DFT methods are significant for the interpretation of the results.

Benchmark plots over the aromaticity indexes calculated for the unrelaxed structures and the other excited manifold are located in the SI. In general, the same tendencies are observed. It is noted, however, that remarkably different index values for all the aromaticity indexes are predicted with the M06-2X functional in the calculations of pyridine on the T_1 surface. This is true for both the unrelaxed and relaxed structures. The Minnesota functional does not include long-range contributions.[27] In comparison, both the CAM-B3LYP and ωB97X-D method include long-range corrections. It is by now a well-established fact, that improper asymptotic behavior of DFT functionals can cause substantial errors, especially in spatially extended π-system.[53–55] The same is observed in the present results. Here, the effect of wrong non-local behavior of the Minnesota functional gets intensified from the S_1 manifold to the T_1 manifold, at which the molecules experience a greater spatial distortion in their π-system and thus display larger differences. Consequently, the observed jumps in index values with respect to the M06-2X method are attributed to the lack of long-range corrections within the functional. This is in line with previous studies of Casademont-Reig et al., in which the admixture of exact exchange was found to be important for electronic- and structural-centered aromaticity descriptors.[34,56] It is noted, on the other hand, that the Minnesota functional predicted the fewest transition structures.

Fig. S6 and S13 in the SI show the HOMA index and AV1245 index for the relaxed

structures within the T_1 manifold, respectively. Negative index values are obtained with the CAM-B3LYP and ωB97X-D level of theories for the pyridine calculations. This is a consequence of the two vertical (see Fig. 1) CC bonds being prolonged with approximately 0.2 Å, when these two DFT functionals are employed. Overall, the CAM-B3LYP and ωB97X-D functionals are found to perform well, and either method can thus be used in combination with the cc-pVTZ basis set for excited state aromaticity calculations. However, since the reference ground state geometries were calculated with the CAM-B3LYP functional, the following assessment of aromaticity is based upon the aromaticity indexes calculated at the CAM-B3LYP/cc-pVTZ level of theory.

3.2 Assessment of Aromaticity

The following assessment is based upon the limit index values presented in paper I.[16,21,57] Table 1 shows the aromaticity indexes calculated at the two electronic excited manifolds with respect to both the relaxed and unrelaxed geometries. It follows from all the aromaticity indexes, except the HOMA index for the relaxed structure on the S_1 surface, that benzene is anti-aromatic. This is in agreement with Baird's rule[10] and the computations by Karadakov.[11] The value of the HOMA index with respect to the relaxed structure within the S_1 manifold, on the other hand, can be assigned to both properties.

Comparison of the aromaticity indexes, with the exception of the AV1245 index, reveals, that both the relaxed and unrelaxed structure of benzene within the S_1 manifold exhibit larger aromatic character compared to the corresponding structures within the T_1 manifold. The AV1245 index, on the other hand, deviates from this trend with respect to the relaxed structure of benzene, as the larger index values are predicted on the T_1 surface. Furthermore, the unrelaxed structure of benzene is observed to be slightly more aromatic than the relaxed structure regardless of the excited manifold. The opposite, however, is observed on the T_1 surface for the AV1245 index.

Table 1: Tabulated aromaticity indexes for benzene calculated with the CAM-B3LYP/cc-pVTZ level of theory.

Manifold	FLU	HOMA	PDI	AV1245	MCI
S_1 (relaxed)	1.15×10^{-2}	0.811	1.49×10^{-2}	0.063	9.44×10^{-3}
S_1 (unrelaxed)	1.03×10^{-2}	-	1.56×10^{-2}	0.071	9.49×10^{-3}
T_1 (relaxed)	2.55×10^{-2}	0.629	1.25×10^{-2}	0.076	6.33×10^{-3}
T_1 (unrelaxed)	2.13×10^{-2}	-	1.35×10^{-2}	0.069	6.95×10^{-3}

The aromaticity indexes for pyridine are tabulated in table 2. The FLU index and MCI predict both structures of pyridine to be of anti-aromatic character on both excited manifolds. In fact, all the aromaticity indexes predict the relaxed and unrelaxed structure on the T_1 surface to be anti-aromatic. The HOMA index, on the other hand, indicates the relaxed structure of pyridine within the S_1 manifold to be aromatic. Both the PDI and AV1245 index are unclear in their interpretation, as each of them can be assigned to both properties. It is noted, however, that their values are close to the associated threshold values for anti-aromaticity, therefore, the results are concluded to predict anti-aromaticity overall. Thereby, the geometrical HOMA index, is observed to result in a different assessment compared to the ESIs. Pyridine has 6 π-electrons, and is thus expected to be anti-aromatic within the T_1 manifold according to Baird's rule. This is encaptured quite well with all the aromaticity indexes.

In regard to the manifold and relaxation dependence on the aromaticity, the same tendencies as described for benzene are observed for pyridine overall. Meanwhile, a significant change in the aromaticity indexes is observed between benzene and pyridine. The two molecules differ in one atom, that is, one carbon atom in benzene is substituted with one nitrogen atom in pyridine. Consequently, the changes in

Table 2: Tabulated aromaticity indexes for pyridine calculated with the CAM-B3LYP/cc-pVTZ level of theory.

Manifold	FLU	HOMA	PDI	AV1245	MCI
S_1 (relaxed)	2.13×10^{-2}	0.910	4.41×10^{-2}	3.119	1.57×10^{-2}
S_1 (unrelaxed)	1.66×10^{-2}	-	4.84×10^{-2}	3.241	1.64×10^{-2}
T_1 (relaxed)	3.77×10^{-2}	-0.642	2.58×10^{-2}	-1.439	3.71×10^{-3}
T_1 (unrelaxed)	2.08×10^{-2}	-	1.54×10^{-2}	0.006	6.58×10^{-3}

aromaticity indexes can be attributed solely to the presence of the nitrogen atom. Vela and Gazquez have calculated the atomic Hückel parameters for the 2p electrons of carbon and nitrogen utilizing extended Hückel theory. The obtained parameters are $\alpha_C = -11.4$ eV and $\alpha_N = -13.4$ eV, respectively.[58] It follows, that the π-electron within the nitrogen's p-orbital is lower in energy compared to the π-electron in the p-orbital of carbon. This means, that the effective coupling between the two π-electrons on adjacent p-orbitals, one from carbon and one from nitrogen, is smaller, and thereby, their interaction is weakened. The smaller effective coupling between the carbon atom and the nitrogen atom, compared to a coupling solely between carbon atoms, accounts for the observed changes in the aromaticity indexes.

Table 3, 4 and 5 show the aromaticity indexes for the diazines, that is, pyridazine, pyrimidine and pyrazine, respectively. Only the FLU indexes and MCIs clearly predict both excited structures of pyridazine to be anti-aromatic. The rest of the aromaticity indexes can be assigned to both properties slightly, although, it is noted, that the HOMA indexes almost predict anti-aromaticity. The same is true for both excited structures of pyrimidine, except for the HOMA indexes, which now indicate aromatic character. The interpretation of the aromaticity indexes for pyrazine is similar to the one for pyrimidine, however, with respect to the former, the MCIs do

Table 3: Tabulated aromaticity indexes for pyridazine calculated with the CAM-B3LYP/cc-pVTZ level of theory.

Manifold	FLU	HOMA	PDI	AV1245	MCI
S_1 (relaxed)	1.47×10^{-2}	0.735	4.84×10^{-2}	1.795	1.21×10^{-2}
S_1 (unrelaxed)	8.33×10^{-3}	-	5.20×10^{-2}	2.425	1.49×10^{-2}
T_1 (relaxed)	1.88×10^{-2}	0.713	4.65×10^{-2}	2.450	1.28×10^{-2}
T_1 (unrelaxed)	8.65×10^{-3}	-	4.48×10^{-2}	3.130	1.66×10^{-2}

not clearly indicate aromaticity or anti-aromaticity.

Table 4: Tabulated aromaticity indexes for pyrimidine calculated with the CAM-B3LYP/cc-pVTZ level of theory.

Manifold	FLU	HOMA	PDI	AV1245	MCI
S_1 (relaxed)	9.21×10^{-3}	0.924	4.54×10^{-2}	2.566	1.60×10^{-2}
S_1 (unrelaxed)	7.98×10^{-3}	-	4.96×10^{-2}	2.452	1.68×10^{-2}
T_1 (relaxed)	1.08×10^{-2}	0.924	4.56×10^{-2}	2.924	1.69×10^{-2}
T_1 (unrelaxed)	8.05×10^{-3}	-	4.94×10^{-2}	2.883	1.79×10^{-2}

In line with the observations for benzene and pyridine, the unrelaxed structures of pyridazine are found to be more aromatic than the corresponding relaxed structures. The PDI at the T_1 surface, however, deviates from this trend, as it predicts the relaxed structure to be more aromatic. Similarly, pyrimidine is predicted to be more aromatic prior to the excited state relaxation with one exception, that is, the AV1245 index, which predicts the relaxed structure to contain more aromatic character on the S_1 surface. The same trend is not observed for pyrazine in general. Here, the

Table 5: Tabulated aromaticity indexes for pyrazine calculated with the CAM-B3LYP/cc-pVTZ level of theory.

Manifold	FLU	HOMA	PDI	AV1245	MCI
S_1 (relaxed)	7.53×10^{-3}	1.000	5.69×10^{-2}	4.147	2.31×10^{-2}
S_1 (unrelaxed)	7.23×10^{-3}	-	5.67×10^{-2}	4.139	2.30×10^{-2}
T_1 (relaxed)	8.94×10^{-3}	0.995	5.94×10^{-2}	4.140	2.33×10^{-2}
T_1 (unrelaxed)	8.67×10^{-3}	-	5.96×10^{-2}	4.156	2.34×10^{-2}

unrelaxed structures are predicted to be more aromatic than the relaxed ones within both manifolds only by the FLU indexes, whereas the PDIs, AV1245 indexes and MCIs only indicate this with respect to the T_1 manifold.

In regard to the electronic manifolds, the more aromatic character for pyridazine is predicted on the S_1 surface with the FLU indexes, HOMA indexes and PDIs. AV1245 and MCI, on the other hand, indicate the opposite. The similar behavior of the AV1245 index and MCI is expected, since the former is defined in terms of the latter.[21] Overall, similar performance is observed for pyrimidine, although it is noted, that the HOMA indexes are identical, and that the interpretation depends upon whether or not the structure is geometrical relaxed. The same is true for pyrazine. Both the FLU index and HOMA index indicate more aromaticity within the S_1 manifold, whereas the MCI and PDI predict the opposite. The AV1245 index predict the T_1 surface to be more aromaticity based upon the unrelaxed geomtries, and vice versa for the relaxed structures.

All the diazines are expected to be anti-aromatic in their electronic T_1 manifold according to Baird's rule. The HOMA index fails to predict such outcomes for pyrimidine and pyrazine. In fact, only the FLU index clearly indicates anti-aromaticity

on the T_1 surface, while the other ESIs in general result in index values that can be assigned to both properties slightly. On the basis of the FLU index, the relative order of aromaticity within the molecules is provided in table 6. It follows, that the ordering on the S_1 and T_1 surfaces with respect to the unrelaxed and relaxed structures, respectively, is identical. The relative ordering with respect to the relaxed structure within the S_1 manifold differs from this trend in terms of the placement of benzene and pyridazine, which has been interchanged. In respect to the unrelaxed structures on the T_1 surface, the relative order of aromaticity has changed. However, inspection of the index values reveals, that the values for pyrimidine, pyridazine and pyrazine are very alike. The same is true for benzene and pyridine.

Table 6: Relative order of aromaticity within the molecules based upon the FLU indexes obtained at the CAM-B3LYP/cc-pVTZ level of theory. The amount of aromaticity decreases from left to right.

Manifold	Relative order of aromaticity								
S_0 (relaxed)[16]	benzene	>	pyridine	>	pyrimidine	>	pyridazine	>	pyrazine
S_1 (relaxed)	pyrazine	>	pyrimidine	>	benzene	>	pyridazine	>	pyridine
S_1 (unrelaxed)	pyrazine	>	pyrimidine	>	pyridazine	>	benzene	>	pyridine
T_1 (relaxed)	pyrazine	>	pyrimidine	>	pyridazine	>	benzene	>	pyridine
T_1 (unrelaxed)	pyrimidine	>	pyridazine	>	pyrazine	>	pyridine	>	benzene

Overall, the relative order of excited state aromaticity is found to be the reversed version of the relative order of ground state aromaticity, which was reported in paper I.[16,59] On the basis of this observation, the following rule is postulated; 'the more aromatic a molecule is in its ground state, the more anti-aromatic it will be in its electronic first excited manifolds'.

4 Conclusion

The aromaticity indexes; HOMA, PDI, MCI, AV1245 and FLU have been benchmarked for their application in excited state aromaticity calculations in this work. In particular, the CAM-B3LYP, ωB97X-D and M06-2X method, each in combination with the 6-31+G(d), cc-pVTZ and Def2TZVP basis set, have been tested. Moreover, the manifold and topological effects on aromaticity have been investigated.

The benchmark study proved the importance of proper long-range behavior in the functional description and high angular momentum polarization basis functions as well as build-in correlation effects in the basis set. Consequently, the long-range corrected CAM-B3LYP and ωB97X-D functionals in combination with the cc-pVTZ basis set were found to give the best results. In addition, basis set augmentation with diffuse functions was concluded to cause little to no effect on the aromaticity indexes. This is in agreement with the findings from paper I.

The aromaticity assessments were based upon the CAM-B3LYP/cc-pVTZ computations. The excited structures of the diazines were in general found to be more aromatic than the corresponding structures of pyridine and benzene. Only the FLU index succeeded in predicting anti-aromatic character for all the molecules as expected based on Baird's rule. The other ESIs mostly resulted in index values that could be assigned to both properties slightly. It was noted, moreover, that the relative order of excited state aromaticity within the tested molecules resembled the reversed version of the relative order of ground state aromaticity. This observation lead to the following generalization; 'the more aromatic a molecule is in its ground state, the more anti-aromatic it will be in its electronic first excited manifolds'. Now, because of the generality represented by the structures in the compound test set, this generalization is expected to be transferable to most polycyclic arenes and heteroarenes. However, its validity should be addressed in more detail in future studies.

In respect to the manifold and topological effects, both the unrelaxed and relaxed

structures displayed in general more aromatic character on the T_1 surface compared to the S_1 surface. Besides, geometrical relaxation on each of the manifolds was found to hamper the aromaticity, thereby resulting in more anti-aromatic character. In the context of artificial photosynthesis and the usage of aromaticity reversal for enhancing switching abilities, the investigated molecules are thus not expected to be promising candidates, since the gain of anti-aromaticity upon photoexcitation is energetic unfavorable.

In conclusion, this study, in combination with the first paper in this series, has presented two computational feasible and reliable procedures for the calculation of aromaticity indexes with respect to ground and first excited states, that is, CAM-B3LYP/cc-pVTZ and ωB97X-D/cc-pVTZ. Future aromaticity calculations are thus strongly recommended to be performed with either one of these two level of theories.

5 Conflict of Interest

The authors declare no conflict of interest.

6 Supporting Information

Tabulated aromaticity indexes, listed imaginary normal mode frequencies with corresponding level of theories, and all benchmark plots.

7 Acknowledgement

The authors thank Peter Søndergaard and PS-DATA for providing computer resources to speed up the wavefunction analyses. The authors, moreover, thanks PhD stud. Nicolai Ree for initial discussions on the topic. Financial support is acknowledged from the European Commission (Grant No. 765739), and the Danish Council for Independent Research, DFF-0136-00081B.

8 References

[1] Fowler, P. W.; Lillington, M.; Olson, L. P. Aromaticity, π-electron delocalization, and ring currents. *Pure Appl. Chem.* **2007**, *79*, 969–979.

[2] Ottosson, H. Exciting excited-state aromaticity. *Nat. Chem.* **2012**, *4*, 969–971.

[3] Cossío, F. P.; Morao, I.; Jiao, H.; Schleyer, P. R. In-plane aromaticity in 1,3-dipolar cycloadditions. Solvent effects, selectivity, and nucleus-independent chemical shifts. *J. Am. Chem. Soc.* **1999**, *121*, 6737–6746.

[4] Katritzky, A. R.; Barczynski, P.; Musumarra, G.; Pisano, D.; Szafran, M. Aromaticity as a quantitative concept. 1. A statistical demonstration of the orthogonality of classical and magnetic aromaticity in five-and six-membered heterocycles. *J. Am. Chem. Soc.* **1989**, *111*, 7–15.

[5] Breslow, R.; Brown, J.; Gajewski, J. J. Antiaromaticity of cyclopropenyl anions. *J. Am. Chem. Soc.* **1967**, *89*, 4383–4390.

[6] Dewar, M. J. S. A molecular orbital theory of organic chemistry—VIII: Aromaticity and electrocyclic reactions. *Tetrahedron* **1966**, *22*, 75–92.

[7] Clayden, J.; Greeves, N.; Warren, S., *Organic Chemistry*; OUP Oxford: (2012).

[8] Portella, G.; Poater, J.; Sola, M. Assessment of Clar's aromatic π-sextet rule by means of PDI, NICS and HOMA indicators of local aromaticity. *J. Phys. Org. Chem.* **2005**, *18*, 785–791.

[9] Rzepa, H. S. Möbius aromaticity and delocalization. *Chem. Rev.* **2005**, *105*, 3697–3715.

[10] Baird, N. C. Quantum organic photochemistry. II. Resonance and aromaticity in the lowest $^3\pi\pi^*$ state of cyclic hydrocarbons. *J. Am. Chem. Soc.* **1972**, *94*, 4941–4948.

[11] Karadakov, P. B. Ground-and excited-state aromaticity and antiaromaticity in benzene and cyclobutadiene. *J. Phys. Chem. A* **2008**, *112*, 7303–7309.

[12] Karadakov, P. B. Aromaticity and antiaromaticity in the low-lying electronic states of cyclooctatetraene. *J. Phys. Chem. A* **2008**, *112*, 12707–12713.

[13] Durbeej, B.; Wang, J.; Oruganti, B. Molecular photoswitching aided by excited-state aromaticity. *ChemPlusChem* **2018**, *83*, 958–967.

[14] Daub, J.; Knöchel, T.; Mannschreck, A. Photosensitive dihydroazulenes with chromogenic properties. *Angew. Chem. Int. Ed. Engl.* **1984**, *23*, 960–961.

[15] Skov, A. B.; Ree, N.; Gertsen, A. S.; Chabera, P.; Uhlig, J.; Lissau, J. S.; Nucci, L.; Pullerits, T.; Mikkelsen, K. V.; Nielsen, M. B.; Sølling, T. I.; Hansen, T. Excited-State Topology Modifications of the Dihydroazulene Photoswitch Through Aromaticity. *ChemPhotoChem* **2019**, *3*, 577–577.

[16] Pedersen, J.; Mikkelsen, K. V. A benchmark study of aromaticity indexes for benzene, pyridine and the diazines–I. Ground state aromaticity. *RSC Adv.* **2022**, *12*, 2830–2842.

[17] Kruszewski, J.; Krygowski, T. M. Definition of aromaticity basing on the harmonic oscillator model. *Tetrahedron Lett.* **1972**, *13*, 3839–3842.

[18] Krygowski, T. M. Crystallographic studies of inter-and intramolecular interactions reflected in aromatic character of π-electron systems. *J. Chem. Inf. Comp. Sci.* **1993**, *33*, 70–78.

[19] Poater, J.; Fradera, X.; Duran, M.; Solá, M. The delocalization index as an electronic aromaticity criterion: application to a series of planar polycyclic aromatic hydrocarbons. *Chem. Euro. J.* **2003**, *9*, 400–406.

[20] Bultinck, P.; Rafat, M.; Ponec, R.; Van Gheluwe, B. V.; Carbo-Dorca, R.; Popelier, P. Electron delocalization and aromaticity in linear polyacenes: atoms in molecules multicenter delocalization index. *J. Phys. Chem. A* **2006**, *110*, 7642–7648.

[21] Matito, E. An electronic aromaticity index for large rings. *Phys. Chem. Chem. Phys.* **2016**, *18*, 11839–11846.

[22] Matito, E.; Duran, M.; Sola, M. The aromatic fluctuation index (FLU): A new aromaticity index based on electron delocalization. *J. Chem. Phys.* **2005**, *122*, 014109.

[23] Matito, E.; Solá, M.; Salvador, P.; Duran, M. Electron sharing indexes at the correlated level. Application to aromaticity calculations. *Faraday Disc.* **2007**, *135*, 325–345.

[24] Feixas, F.; Matito, E.; Poater, J.; Solà, M. On the Performance of Some Aromaticity Indices: A Critical Assessment Using a Test Set. *J. Comput. Chem.* **2008**, *29*, 1543–1554.

[25] Chai, J.; Head-Gordon, M. Long-range corrected hybrid density functionals with damped atom–atom dispersion corrections. *Phys. Chem. Chem. Phys.* **2008**, *10*, 6615–6620.

[26] Yanai, T.; Tew, D. P.; Handy, N. C. A new hybrid exchange–correlation functional using the Coulomb-attenuating method (CAM-B3LYP). *Chem. Phys. Lett.* **2004**, *393*, 51–57.

[27] Zhao, Y.; Truhlar, D. G. The M06 suite of density functionals for main group thermochemistry, thermochemical kinetics, noncovalent interactions, excited states, and transition elements: two new functionals and systematic testing of four M06-class functionals and 12 other functionals. *Theo. Chem. Acc.* **2008**, *120*, 215–241.

[28] Lennartson, A.; Roffey, A.; Moth-Poulsen, K. Designing photoswitches for molecular solar thermal energy storage. *Tetrahedron Lett.* **2015**, *56*, 1457–1465.

[29] Nielsen, M. B.; Ree, N.; Mikkelsen, K. V.; Cacciarini, M. Tuning the dihydroazulene–vinylheptafulvene couple for storage of solar energy. *Russ. Chem. Rev.* **2020**, *89*, 573.

[30] Kilde, M. D.; Mansø, M.; Ree, N.; Petersen, A. U.; Moth-Poulsen, K.; Mikkelsen, K. V.; Nielsen, M. B. Norbornadiene–dihydroazulene conjugates. *Org. Bio. Chem.* **2019**, *17*, 7735–7746.

[31] Bader, R. F. W. Molecular fragments or chemical bonds. *Acc. Chem. Res.* **1975**, *8*, 34–40.

[32] Bader, R. F. W. Atoms in molecules. *Acc. Chem. Res.* **1985**, *18*, 9–15.

[33] Strogatz, S. H., *Nonlinear Dynamics and Chaos*; CRC press: (2018).

[34] Casademont-Reig, I.; Woller, T.; Contreras-Garcıa, J.; Alonso, M.; Torrent-Sucarrat, M.; Matito, E. New electron delocalization tools to describe the aromaticity in porphyrinoids. *Phys. Chem. Chem. Phys.* **2018**, *20*, 2787–2796.

[35] Frisch, M. J.; Trucks, G. W.; Schlegel, H. B.; Scuseria, G. E.; Robb, M. A.; Cheeseman, J. R.; Scalmani, G.; Barone, V.; Petersson, G. A.; Nakatsuji, H.; Li, X.; Caricato, M.; Marenich, A. V.; Bloino, J.; Janesko, B. G.; Gomperts, R.; Mennucci, B.; Hratchian, H. P.; Ortiz, J. V.; Izmaylov, A. F.; Sonnenberg, J. L.; Williams-Young, D.; Ding, F.; Lipparini, F.; Egidi, F.; Goings, J.; Peng, B.; Petrone, A.; Henderson, T.; Ranasinghe, D.; Zakrzewski, V. G.; Gao, J.; Rega, N.; Zheng, G.; Liang, W.; Hada, M.; Ehara, M.; Toyota, K.; Fukuda, R.; Hasegawa, J.; Ishida, M.; Nakajima, T.; Honda, Y.; Kitao, O.; Nakai, H.; Vreven, T.; Throssell, K.; Montgomery J. A., J.; Peralta, J. E.; Ogliaro, F.; Bearpark, M. J.; Heyd, J. J.; Brothers, E. N.; Kudin, K. N.; Staroverov, V. N.; Keith, T. A.; Kobayashi, R.; Normand, J.; Raghavachari, K.; Rendell, A. P.; Burant, J. C.; Iyengar, S. S.; Tomasi, J.; Cossi, M.; Millam, J. M.; Klene, M.; Adamo, C.; Cammi, R.; Ochterski, J. W.; Martin, R. L.; Morokuma, K.; Farkas, O.; Foresman, J. B.; Fox, D. J. Gaussian 16 Revision A.03, Gaussian, Inc. Wallingford, CT, 2016.

[36] Olsen, J.; Jørgensen, P. Linear and nonlinear response functions for an exact state and for an MCSCF state. *J. Chem. Phys.* **1984**, *82*, 3235–3264.

[37] Dalgaard, E. Time-dependent multiconfigurational Hartree–Fock theory. *J. Chem. Phys.* **1980**, *72*, 816–823.

[38] Dalgaard, E. Quadratic response functions within the time-dependent Hartree-Fock approximation. *Phys. Rev. A* **1982**, *26*, 42.

[39] Sałek, P.; Vahtras, O.; Helgaker, T.; Ågren, H. Density-functional theory of linear and nonlinear time-dependent molecular properties. *J. Chem. Phys.* **2002**, *117*, 9630–9645.

[40] Olsen, J.; Jørgensen, P.; Helgaker, T.; Oddershede, J. Quadratic response functions in a second-order polarization propagator framework. *J. Phys. Chem. A* **2005**, *109*, 11618–11628.

[41] Pedersen, J.; Mikkelsen, K. V. Working equation of linear response time-dependent density functional theory: First-order polarization propagator approximation. *Int. J. Quantum Chem.* **2022**, *122*, e26891.

[42] Dunning Jr, T. H. Gaussian basis sets for use in correlated molecular calculations. I. The atoms boron through neon and hydrogen. *J. Chem. Phys.* **1989**, *90*, 1007–1023.

[43] Woon, D. E.; Dunning Jr, T. H. Gaussian basis sets for use in correlated molecular calculations. III. The atoms aluminum through argon. *J. Chem. Phys.* **1993**, *98*, 1358–1371.

[44] Weigend, F.; Ahlrichs, R. Balanced basis sets of split valence, triple zeta valence and quadruple zeta valence quality for H to Rn: Design and assessment of accuracy. *Phys. Chem. Chem. Phys.* **2005**, *7*, 3297–3305.

[45] Krishnan, R. B. J. S.; Binkley, J. S.; Seeger, R.; Pople, J. A. Self-consistent molecular orbital methods. XX. A basis set for correlated wave functions. *J. Chem. Phys.* **1980**, *72*, 650–654.

[46] Frisch, M. J.; Pople, J. A.; Binkley, J. S. Self-consistent molecular orbital methods 25. Supplementary functions for Gaussian basis sets. *J. Chem. Phys.* **1984**, *80*, 3265–3269.

[47] Todd, A. K. AIMAll (Version 19.10.12), TK Gristmill Software, Overland Park KS, USA, aim.tkgristmill.com, 2019.

[48] Matito, E. ESI-3D: Electron Sharing Indexes Program for 3D Molecular Space Partitioning, Institute of Computational Chemistry and Catalysis (IQCC), University of Girona, Catalonia, Spain, http://iqc.udg.es/∼eduard/ESI, 2006.

[49] Raffenetti, R. C. General contraction of Gaussian atomic orbitals: Core, valence, polarization, and diffuse basis sets; Molecular integral evaluation. *J. Chem. Phys.* **1973**, *58*, 4452–4458.

[50] Jensen, F. Unifying general and segmented contracted basis sets. Segmented polarization consistent basis sets. *J. Chem, Theory Comput.* **2014**, *10*, 1074–1085.

[51] Almlöf, J.; Taylor, P. R. General contraction of Gaussian basis sets. I. Atomic natural orbitals for first- and second-row atoms. *J. Chem. Phys.* **1987**, *86*, 4070–4077.

[52] Almlöf, J.; Helgaker, T.; Taylor, P. R. Gaussian Basis Sets for High-Quality ab Initio Calculations. *J. Phys. Chem.* **1988**, *92*, 3029–3033.

[53] Dreuw, A.; Weisman, J. L.; Head-Gordon, M. Long-range charge-transfer excited states in time-dependent density functional theory require non-local exchange. *J. Chem. Phys.* **2003**, *119*, 2943–2946.

[54] Tozer, D. J.; Amos, R. D.; Handy, N. C.; Roos, B. O.; Serrano-Andres, L. Does density functional theory contribute to the understanding of excited states of unsaturated organic compounds? *Mol. Phys.* **1999**, *97*, 859–868.

[55] Cai, Z.-L.; Sendt, K.; Reimers, J. R. Failure of density-functional theory and time-dependent density-functional theory for large extended π systems. *J. Chem. Phys.* **2002**, *117*, 5543–5549.

[56] Casademont-Reig, I.; Ramos-Cordoba, E.; Torrent-Sucarrat, M.; Matito, E. How do the Hückel and Baird rules fade away in annulenes? *Molecules* **2020**, *25*, 711.

[57] Papadakis, R.; Ottosson, H. The excited state antiaromatic benzene ring: a molecular Mr Hyde? *Chem. Soc. Rev.* **2015**, *44*, 6472–6493.

[58] Vela, A.; Gazquez, J. L. Extended Hückel parameters from density functional theory. *J. Phys. Chem.* **1988**, *92*, 5688–5693.

[59] Bures, M. G.; Roos-Kozel, B. L.; Jorgensen, W. L. Computer-assisted mechanistic evaluation of organic reactions. 11. Electrophilic aromatic substitution. *J. Org. Chem.* **1985**, *50*, 4490–4498.

9 TOC Graphic